Journal of Molecular Structure 1133 (2017) 436–447

Contents lists available at ScienceDirect

Journal of Molecular Structure

journal homepage: http://www.elsevier.com/locate/molstruc

Synthesis and characterization of a series of isoniazid hydrazones. Spectroscopic and theoretical study

Verónica Ferraresi-Curotto [a], Gustavo A. Echeverría [b], Oscar E. Piro [b], Reinaldo Pis-Diez [a], Ana C. González-Baró [a, *]

[a] CEQUINOR (CONICET, UNLP), CC 962, B1900AVV, La Plata, Argentina
[b] IFLP (CONICET, UNLP), CC 67, B1900AVV, La Plata, Argentina

ARTICLE INFO

Article history:
Received 21 June 2016
Received in revised form
17 November 2016
Accepted 5 December 2016
Available online 9 December 2016

Keywords:
Crystal structures
Spectroscopy
DFT calculations
Isoniazid
Schiff bases

ABSTRACT

A family of hydrazones of isoniazid and a group of hydroxybenzalaldehydes (vanillin, 5-bromovanillin, 5-chlorosalicylaldehyde and 5-bromosalicylaldehyde) were obtained and fully characterized. The results, including theoretical data, are comparatively analyzed along with the already reported hydrazone of *o*-vanillin. The crystal structures of three compounds were determined. The hydrazones obtained from halogenated aldehydes are isomorphic and chiral to each other. Structures are further stabilized by (pyr)$NH^{+}\cdots Cl^{-}$ and $OwH\cdots Cl^{-}$ bonds. The vanillin hydrazone shows a conformer that differs from the previously reported. Neighboring molecules are linked to each other through OH···N(pyr) bonds, giving rise to a nearly planar polymeric structure. The conformational space was searched and geometries were optimized both in the gas phase and including solvent effects by DFT. Results are extended to describe the 5-bromovanillin hydrazone. FTIR, NMR and electronic spectra were measured and assigned with the help of computational calculations.

1. Introduction

The hydrazone functional group has been extensively studied [1 and references therein]. Hydrazones play important roles in various fields, from organic synthesis and medicinal chemistry to supramolecular chemistry, and have many applications. The straightforward synthesis, the possibility of including different substituents, and the stability towards hydrolysis of hydrazones can be cited as reasons for their attractiveness.

The chemical versatility of hydrazones can be mainly attributed to the functional diversity of the azomethine group, particularly the C═N–N moiety. The structure of a hydrazone shows (i) nucleophilic imine and amino-type (more reactive) nitrogens, (ii) an imine carbon that has both electrophilic and nucleophilic character, (iii) configurational isomerism stemming from the intrinsic nature of the C═N double bond, and (iv) in most cases an acidic N–H proton. These structural motifs determines the physical and chemical properties of the hydrazone, playing a crucial role in its applications.

Hydrazones are usually obtained by condensation of one hydrazine or hydrazide with a ketone or aldehyde. The hydrazide here employed is isoniazid, the hydrazide of isonicotinic acid (INH, see Fig. 1). It has been recognized as an effective antituberculous agent and it is still employed in the treatment and prevention of this disease. However, actual formulations containing INH show several undesired side effects. On the other hand, it has been determined that hydrazones obtained from the condensation of isoniazid and some hydroxy-aldehydes are less toxic while preserving activity. This fact can be attributed to the inactivation of the NH_2 group of INH upon hydrazone formation [2 and references therein]. Moreover, hydrazones from INH are interesting chemical systems because they possess an additional nucleophilic cite, the pyridine nitrogen atom.

As part of our study on Schiff base formation with aromatic hydroxy-aldehydes [2,3], a complete study of a family of hydrazones of INH was carried out with a group of aldehydes depicted in Fig. 2, including vanillin (4-hydroxy-3-methoxybenzaldehyde, *Va*) and its derivative 3-bromo-4-hydroxy-5-methoxybenzaldehyde (5-bromovanillin, *BrVa*). Two derivatives of salicylaldehyde are also included, namely 5-chloro-2-hydroxybenzaldehyde (5-chlorosalicylaldehyde, *ClSal*) and 5-bromo-2-hydroxybenzaldehyde (5-bromosalicylaldehyde, *BrSal*).

* Corresponding author.
E-mail address: agb@quimica.unlp.edu.ar (A.C. González-Baró).

http://dx.doi.org/10.1016/j.molstruc.2016.12.018
0022-2860/

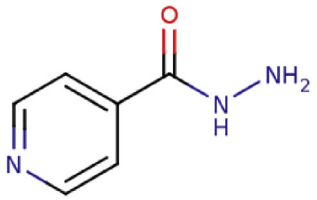

Fig. 1. Structure of isoniazid.

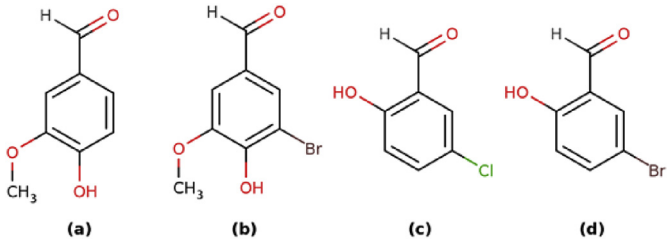

Fig. 2. Structure of the hydroxyl-aldehydes. (**a**) vanillin, (**b**) Br-vanillin, (**c**) 5-chlorosalicylaldehyde, (**d**) 5-bromosalicylaldehyde.

The present article involves a complete experimental and theoretical characterization of the four hydrazones and the comparative analyses with the hydrazone of *o*-vanillin (2-hydroxy-3-methoxybenzaldehyde, *o-HVa*) and INH, INHoVa, already reported by our group (Fig. 3) [2].

For the compounds which afforded suitable single crystals the solid state structures were determined by X-ray diffraction methods. A detailed analysis of inter- and intra-molecular H-bonds is conducted to explain their effects on structure stabilization. FTIR, NMR and electronic absorption spectra were recorded and assigned with the assistance of results from computational methods based on the Density Functional Theory (DFT).

2. Experimental section

2.1. General procedure for the synthesis of isonicotinoyl Schiff bases

The compounds were synthesized according to an adaptation of the reported procedure for the analytical determination of isoniazid with Va [4]. Twenty milliliters of an ethanolic solution containing 3 mmol of the aldehyde (Sigma) was drop-wise added to a solution of 1.5 mmol of isoniazid (Sigma) in ten mL of ethanol (Merck), with continuous stirring and slight heating. Excess of aldehyde has been already employed in previous work [2] as allows obtaining the products in milder experimental conditions, avoiding reflux or long-time heating at high temperature, and have shown to improve the yield. Drops of concentrated hydrochloric acid (Merck) were added to reach a pH value of 5. Upon standing, the products were obtained and the solids were filtered out from the solution, washed repeatedly with cold ethanol and then dried in a desiccator. Melting points were determined using a Bock monoscop "M" instrument as an additional criterion of the products purity.

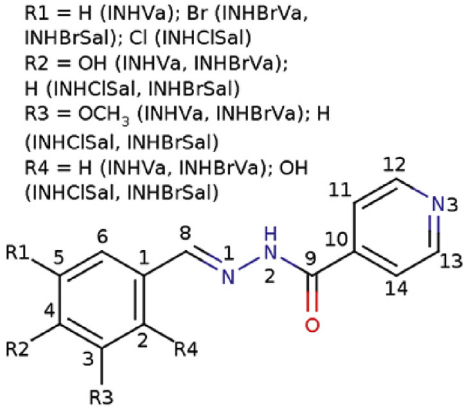

Fig. 3. Structure of the obtained hydrazones.

It is worth mentioning at this point that the hydrazone obtained by the condensation reaction of INH with vanillin (INHVa) has been previously reported by other authors [5] following a different synthetic method and the crystal structure of a different conformer was already reported in the form of a monohydrate [6]. Furthermore, the compound resulting from the condensation reaction of INH with ClSal was already obtained by other authors in different conditions of synthesis [7,8], but no crystal structure was reported.

INHVa (1): (E)-N′-(4-hydroxy-3-methoxybenzylidene) isonicotinohydrazide.

Orange solid precipitated immediately, it was further recristalized from ethanol and yellow prismatic crystals were obtained after a week (m. p. 260–263 °C).

INHBrVa (2): (E)-N′-(3-bromo-4-hydroxy-5-methoxybenzaldehyde)isonicotinohydrazide.

Orange solid not suitable for structural X-ray diffraction study precipitated after two days (m. p. 285–287 °C).

INHClSal (3): (E)-N′-(5-chloro-2-hydroxybenzaldehyde) isonicotinohydrazide.

Colorless thin prismatic crystals suitable for X-ray diffraction were obtained after eleven days (m. p. 246–248 °C).

INHBrSal (4): (E)-N′-(5-bromo-2-hydroxybenzaldehyde) isonicotinohydrazide.

Yellow crystals suitable for structural X-ray diffraction study were obtained after 24 h (m. p. 259–261 °C).

2.2. X-ray diffraction data

The measurements were performed on an Oxford Xcalibur Gemini, Eos CCD diffractometer with graphite-monochromated CuKα (λ = 1.54178 Å) radiation. X-ray diffraction intensities were collected (ω scans with ϑ and κ-offsets), integrated and scaled with CrysAlisPro [9] suite of programs. The unit cell parameters were obtained by least-squares refinement (based on the angular setting for all collected reflections with intensities larger than seven times the standard deviation of measurement errors) using CrysAlisPro. Data were corrected empirically for absorption employing the multi-scan method implemented in CrysAlisPro. The structures were solved by direct methods with SHELXS of the SHELX package [10] and the molecular model developed by alternated cycles of Fourier methods and full-matrix least-squares refinement with SHELXL of the same suit of programs. The H-atoms were found at approximated positions in a difference Fourier map phased on the heavier atoms. However, all but the hydroxyl and water hydrogen atoms were located stereo-chemically and refined with the riding model. The hydroxyl and the water hydrogen atoms were refined at their found positions with isotropic displacement parameters.

The closely related chemical formula, the same space group and almost identical cell constant values strongly suggested that the bromine-containing solid was isomorphic to the chlorine-containing one. In fact, an initial molecular model assuming the same atom positions as in the chlorine crystal with the identity of the ring halogen atom changed from chlorine to bromine, lead to smooth convergence of the structural parameters for the bromide crystal during the least-squares refinement against the corresponding X-ray data set. Interestingly, the Flack's absolute structure

parameter [11] (x) turned out to be x = 1.01(3) thus, indicating that the bromine crystal was the chiral counterpart of the chlorine one. In fact, by inverting the molecular model, the x-value dropped to −0.03(2). The Flack's parameter is the fractional contribution to the diffraction pattern due to the molecule's racemic twin and for the correct enantiomeric crystal it should be zero to within experimental error [10].

Crystal data and structure refinement results are summarized in Table 1.

2.3. Spectroscopic analysis

The FTIR spectra were obtained with a Bruker EQUINOX 55 spectrometer in KBr discs with 4 cm^{-1} resolution and 60 scans, in the 4000–400 cm^{-1} range. ^{1}H-NMR and ^{13}C-NMR spectra were recorded as DMSO-d_6 solutions, on a Bruker Advance II spectrometer at 500 MHz using tetramethylsilane as the internal reference. Electronic absorption spectra were measured on ethanolic 3×10^{-5} M solutions in the 200–800 nm region, with a Hewlett-Packard 8452-A diode array spectrometer using 10 mm quartz cells.

2.4. Computational methods

The conformational space of the compounds was explored with the aid of the semiempirical PM6 method [12]. Several starting geometries derived from selected variations in C14–C10–C9–N2, C10–C9–N2–N1, N2–N1–C8–C1 and N1–C8–C1–C6 torsion angles were optimized (see Fig. 3 for atom labelling). Geometries obtained from X-ray diffraction were also used as a starting point for the optimizations. The geometries were further re-optimized both in gas phase and including solvent effects using the hybrid *meta*-GGA M06–2X exchange–correlation density functional [13] with a triple-zeta 6–311G(d,p) basis set [14,15]. Solvent effects (ethanol) were included implicitly through the Conductor-like Polarizable Continuum Model [16,17]. Numerical integrations were carried out using a grid containing 96 radial points and 590 angular points around each atom. For compounds that involve Br atom [INHBrVA (**2**) and INHBrSal (**4**)], a grid with 160 radial points and 974 angular points was used. The critical points found after optimization were characterized by the sign of the eigenvalues of the Hessian matrix of the total electronic energy with respect to the nuclear coordinates. When the critical point corresponded to a minimum on the potential energy surface, the eigenvalues were converted to harmonic vibrational frequencies. Vibration frequencies were scaled by a factor of 0.982 to ease the comparison with experimental values [13]. Electronic transitions were calculated within the framework of the Time-Dependent DFT (TD-DFT) [18,19] using the PBE0 functional [20] and the triple zeta 6-311+G(d,p) basis set [14,15], with solvent effects, as was previously stated. Geometry optimizations, Hessian matrix calculation and diagonalization, and electronic transition calculations were performed with the GAMESS-US program [21]. Isotropic magnetic shieldings of ^{13}C and ^{1}H were calculated at the B3LYP/6–311+G(2d,p)//B3LYP/6–31G* level of theory as suggested by Cheeseman and co-workers, using the Gauge-independent Atomic Orbital method [22–24]. Isotropic magnetic shieldings were turned into chemical shifts by subtracting the corresponding isotropic magnetic shieldings of TMS, which were calculated at the same

Table 1
Crystal data and structure refinement results for (E)-N′-(5-X-2-hydroxybenzaldehyde) isonicotinohydrazide chloride hydrate (X = Cl, Br) and (E)-N-(4-hydroxy-3-methoxybenzylidene) isonicotinohydrazide hydrate.

Compound	INHVa (**1**)	INHClSal (**3**)	INHBrSal (**4**)
Empirical formula	$C_{14}H_{15}N_3O_4$	$C_{13}H_{13}Cl_2N_3O_3$	$C_{13}H_{13}BrClN_3O_3$
Formula weight (g/mol)	289.29	330.16	374.62
Temperature (K)	293(2)	295(2)	295(2)
Wavelength (Å)	1.54184	1.54184	1.54184
Crystal system	Monoclinic	Orthorhombic	Orthorhombic
Space group	$P2_1/n$	$P2_12_12_1$	$P2_12_12_1$
unit cell dimensions			
a (Å)	8.3741(6)	6.7061(2)	6.7021(1)
b (Å)	13.103(1)	13.5765(6)	13.6568(3)
c (Å)	12.683(2	15.8941(5)	15.9769(3)
β (°)	99.02(1)		
volume (Å^3)	1374.4(2)	1447.08(9)	1462.35(5)
Z, calc. dens. (Mg/m^3)	4, 1.398	4, 1.515	4, 1.702
Abs. Coeff. (mm^{-1})	0.874	4.171	5.648
F(000)	608	680	752
Crystal shape/color	Plate/yellow	Prism/colorless	Prism/yellow
Crystal size (mm^3)	0.269 × 0.178 x 0.015	0.793 × 0.148 x 0.074	0.581 × 0.086 x 0.066
θ-range(°) for data collection	4.88 to 70.96	4.28 to 73.31	4.26 to 71.52
Index ranges	$-10 \le h \le 10$, $-16 \le k \le 14$, $-15 \le l \le 13$	$-3 \le h \le 8$, $-15 \le k \le 16$, $-19 \le l \le 17$	$-8 \le h \le 5$, $-16 \le k \le 16$, $-19 \le l \le 16$
Reflections collected	5778	3768	4195
Independent reflections	2638 [R(int) = 0.0417]	2610 [R(int) = 0.0216]	2426 [R(int) = 0.0161]
Observed reflections [I > 2σ(I)]	1320	2329	2308
Completeness (%)	99.5 (to ϑ = 70.96°)	98.4 (to ϑ = 73.31°)	99.1. (to ϑ = 73.31°)
Max. and min. transmission		0.7589 and 0.5735	0.6932 and 0.1472
Refinement method	Full-matrix least-squares on F^2	Full-matrix least-squares on F^2	Full-matrix least-squares on F^2
Data/restraints/parameters	2638/3/203	2610/0/202	2426/0/203
Goodness-of-fit on F^2	1.018	1.041	1.047
Final R indices[a] [I > 2σ(I)]	R1 = 0.0578, wR2 = 0.1171	R1 = 0.0402, wR2 = 0.1075	R1 = 0.0289, wR2 = 0.0762
R indices (all data)	R1 = 0.1217, wR2 = 0.1597	R1 = 0.0452, wR2 = 0.1123	R1 = 0.0304, wR2 = 0.0776
Absolute structure parameter		0.00(2)	−0.03(2)
Larg. diff. peak & hole (e.Å^{-3})	0.146 and −0.191	0.217 and −0.265	0.306 and −0.272

[a] $R_1 = \Sigma||F_o|-|F_c||/\Sigma|F_o|$, $wR_2 = [\Sigma w(|F_o|^2-|F_c|^2)^2/\Sigma w(|F_o|^2)^2]^{1/2}$.

level of theory as above. Solvent effects (DMSO) were included implicitly through the Integral Equation Formalism version of the Polarizable Continuum Model [25]. Isotropic magnetic shieldings were calculated with the Gaussian 03 package [26]. The animation of the vibrational modes was done with Gabedit [27] and MO's figures were done with wxMacMolPlt [28]. Potential energy distribution analyses were carried out with the program vibca [29]. Marvin was used for drawing chemical structures [30]. Chloride counter-ion and water molecules present in the crystals were not considered in the calculations.

3. Results and discussion

3.1. Crystallographic structural data

Crystal data and structure refinement results are summarized in Table 1 for all compounds which were suitable for crystallographic analyses.

3.1.1. (E)-N′-(4-hydroxy-3-methoxybenzylidene) isonicotinohydrazide hydrate: INHVa (**1**)

Fig. 4 shows an ORTEP [31] drawing of the solid state structure and corresponding intra-molecular bond distances and angles are listed in the Supplementary Material, Table S1a. The organic molecule is nearly planar [*rms* deviation of non-H atoms from the best least-squares molecular plane of 0.044 Å] and closely related to the isomorphic pair (**3**) and (**4**). In fact, it can be obtained from these latter molecules by replacing the halide-substituents for a methoxy group and changing the location of the hydroxyl group from 2- to 4- position in the ring. The pyridine moiety is deprotonated, rendering the conformer electrically neutral. The main structural differences between (**1**) and the pair (**3**) and (**4**) include: (i) a shortening of the mean pyridine C—N bond length of 0.011 Å upon deprotonation and (ii) the removal of the intra-molecular OH···N bond in the isomorphic compounds and the formation of a bent OH···O(methoxy) new bond in the conformer [d(OH···O) = 2.237 Å and ∠ (O—H···O) = 108.0°].

The molecular structure of a quite different conformer, also crystallized as monohydrate in the same space group $P2_1/n$, having nearly the same volume but in a different unit cell, has been reported [6]. In fact, the conformers are nearly related to each other through a rotation of about 180° around the Ph-C σ-bond (C1—C8 bond in Fig. 4). Though showing a good agreement in bond distances and angles, the reported one further differs from the presented here in its appreciable deviation from planarity. As expected, the conformer crystals also differ from each other in their packing.

The mentioned differences between both conformers can be a consequence of different experimental conditions in the preparation. In the present work the crystals were obtained by letting the recrystallization solution slowly cool to room temperature and then keeping it for at least one week. The previously reported procedure describes a faster cooling followed by the separation of the product from the solution. The anhydrate of this latter conformer has been reported to crystallize in the *Cc* space group [32] and the structure of yet another closely related conformer that crystallizes in the $P2_1/c$ space group with a methanol solvent molecule has also been published [33].

Hydrogen bond distances and angles are detailed in Table S2a of the Supplementary Material. The crystal is further stabilized by inter-molecular H-bonds. Neighboring molecules are linked to each other through OH···Npyr bonds [d(OH···N) = 1.806 Å and ∠ (O—H···N) = 149.6°] giving rise to a nearly planar, ribbon-like, polymeric structure that extends along the crystal [-3, 0, 1] direction. In turn, neighboring polymers in the lattice are bridged by the water molecule (nearly onto the molecular plane) through N—H···Ow-H1···O'carb [d(NH … Ow) = 2.135 Å and ∠ (N—H···Ow) = 166.7°; d(OwH1···O'carb) = 1.997 Å and ∠ (Ow-H1···O'carb) = 168.2°] and NH.Ow-H2···O″ox [d(OwH1···O″ox) = 2.247 Å and ∠ (Ow-H1···O″ox) = 143.3°] bonds (see Fig. 4).

3.1.2. (E)-N′-(5-X-2-hydroxybenzaldehyde)isonicotinhydrazide (X: Cl, Br) chloride hydrate: INHClSal (**3**) y INHBrSal (**4**)

As detailed in the experimental section, the solid state compounds are isomorphic and chiral counterparts of each other, differing only in the interchange of chlorine and bromine atoms in the aldehyde ring. In fact, the *rms* separation between homologous non-H atoms in the best least-squares structural fitting of the organic molecules, calculated by the Kabsh's procedure [34] is 0.037 Å (0.018 Å excepting the ring halogen atoms) and involves an improper relative rotation (determinant equal to −1) around the

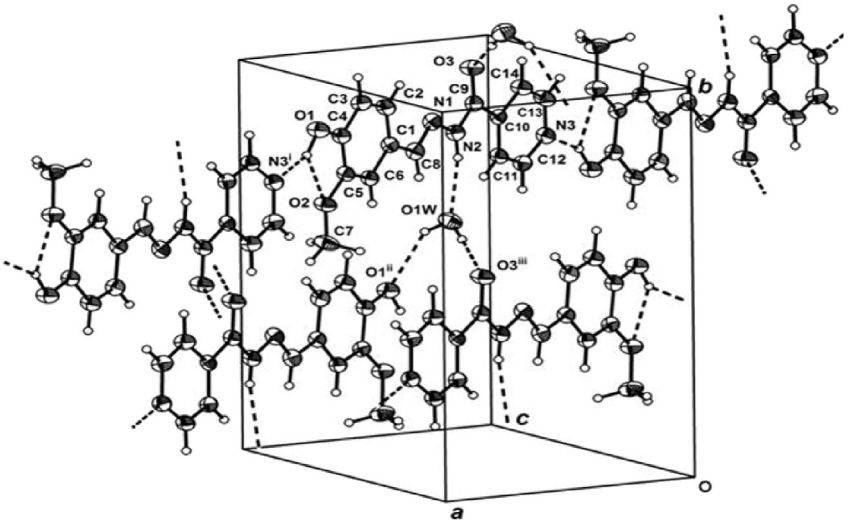

Fig. 4. View of (E)-N′-(4-hydroxy-3-methoxybenzylidene)isonicotinohydrazide hydrate crystal (**1**), showing the labelling of the non-H atoms and their displacement ellipsoids at the 30% probability level. Intra- and inter-molecular H-bonds are indicated by dashed lines.

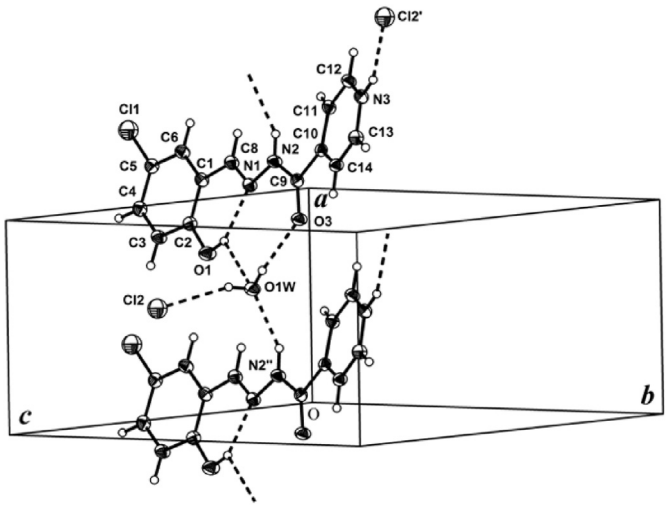

Fig. 5. View of the chlorine-containing member of the (E)-N′-(5-X-2-hydroxybenzaldehyde)isonicotinohydrazide (X: Cl, Br) chloride hydrate isomorphic pair (**3**) and (**4**).

common molecular centroid. Fig. 5 is an ORTEP [31] drawing of the chlorine-containing crystal. The corresponding intra-molecular bond distances and angles for both compounds are listed in the Supplementary Material, Tables S1b and c.

Due in part to delocalized π-bonding, the 5-X-2-hydroxyphenylidene (X = Cl, Br) fragments are nearly planar [*rms* deviation of non-H atoms from the best least-squares plane is less than 0.035 Å for (**3**) and 0.036 Å for (**4**)]. As shown in Fig. 5, the planarity affords the formation of an intra-molecular OH···N bond [OH···N bond distances of 2.012 Å (**3**) and 2.064 Å (**4**), O–H···N angles of 147.2° (**3**) and 145.41° (**4**)]. As expected, the positively charged pyridine moiety is also planar [*rms* deviation of atoms from the plane of 0.015 Å (**3**), 0.014 Å (**4**)] and therefore the only degrees of freedom left to define the molecular conformation are unhindered rotations around the C1–C8, N1–N2, N2–C9, and C9–C10 σ-bonds. In fact, the chiral organic conformers are related to each other mainly through a change of 32.9(3)° in the torsion angle around C9–C10 bond.

Observed intra-molecular bond distances and angles are in agreement with the Organic Chemistry's rules. In particular, C–C distances within the phenyl ring [in the 1.368(4)-1.414(4) Å (**3**) and 1.375(4)-1.402(4) Å (**4**) ranges] are as expected for phenyl resonant-bond structures. C-X bond distances are 1.743(3) Å (**3**) and 1.901(3) Å (**4**). The short imino C8–N1 length [1.267(4) Å (**3**) and 1.268(4) Å (**4**)] contrasts with the longer amido C9–N2 value [1.339(4) Å (**3**) and 1.345(4) Å (**4**)], clearly confirming the formally double and single bond character for these links, respectively. The distance of N–N single bond linking the 5-X-2-hydroxyphenylidene and pyridincarbonylic molecular fragments is 1.388(3) Å (**3**) and 1.396(3) Å (**4**). C–OH and C=O bond distances of 1.349(4) Å (**3**) and 1.355(4) Å (**4**), and 1.223(4) Å (**3**) and 1.217(4) Å (**4**) are the expected for the single and double character of these bonds, respectively. C–N bond lengths within the pyridinium group are 1.340(4) and 1.330(4) Å (**3**), and 1.336(4) and 1.329(4) Å (**4**). Bond distances in the bromide-containing organic cation are in general agreement with the corresponding ones reported in the literature for the neutral (deprotonated) moiety [35,36].

The crystals are further stabilized by (pyr)$NH^{+}\cdots Cl^{-}$ and $OwH\cdots Cl^{-}$ bonds. The water molecule also bridges neighboring organic molecules acting as donor in a OwH···O(carb) bond and as acceptor in a PhOH···Ow bond with a given organic molecule and as acceptor in a NH···Ow bond with another one (see Fig. 5). Hydrogen bond distances and angles for both compounds are detailed in the Supplementary Material, Tables S2b and c.

3.2. Conformational analysis and geometry optimization

As it was previously mentioned, calculations were done using M06-2X functional and 6-311G(d,p) basis set in the gas phase and including solvent effects, as described in the experimental section.

In the case of (**1**), the conformational searching shows that one structure is more stable than other conformations by more than 4 kcal mol^{-1}, both in the gas phase and after including solvent effects. Even the conformation optimized from the X-ray structure is found to be well above in energy than the lowest-energy conformation. For (**3**), the conformational searching in the gas phase shows that one conformation is more stable than other conformations by about 3 kcal mol^{-1}, whereas the conformation optimized from the X-ray structure becomes the more stable one by about 1 kcal mol^{-1} after including solvent effects. Interestingly, (**4**) exhibits a very similar behaviour. A conformation is more stable than others by more than 1 kcal mol^{-1} in the gas phase, whereas the conformation optimized from the X-ray structure becomes the more stable one by about 2 kcal mol^{-1} when solvent effects are taken into account. Finally, in the case of (**2**), for which no experimental structure is known, the conformational searching leads to optimized geometries that become the more stable ones by more than 3 kcal mol^{-1} both in the gas phase and after including solvent effects. From now on, the lowest-energy conformations obtained after including solvent effects are used both for the comparison of geometrical parameters with those structures obtained by X-ray diffraction methods and for the calculation of electronic transitions that aid in the assignment of the electronic spectra. On the other hand, gas-phase lowest-energy conformations are used to calculate harmonic vibrational frequencies that are useful in the assignment of experimental vibrational spectra.

A selection of calculated geometrical parameters is listed in Table 2. Experimental values for those structures that were characterized by X-ray diffraction methods and structural data calculated for (**2**) are included for comparison. It is appreciated from the table that the intra-molecular N1···HO1 bond is overestimated by the calculations in both salicylaldehyde derivatives (**3**) and (**4**). In addition, C–H distances are also slightly overestimated by the calculations. Nonetheless, there is excellent agreement between experimental and theoretical results regarding C–O, C–Cl and C–Br bond distances. It is worth noting that interatomic distances obtained by optimizing with solvent effects for (**2**) agree very well with those obtained for (**1**) and that C–Br bond distance in (**2**) shows almost the same value as the ones found both experimentally and theoretically for (**4**). Calculated bond and torsion angles are also in agreement with those obtained by X-ray diffraction methods and calculated values for (**2**) are very close to those obtained for the other hydrazones. Regarding bond angles, calculated values are in excellent accordance with experimental results (see Table 2). It is worth noticing that the angle formed by –OH with the oxygen atom from OCH_3 substituent in vanillin derivatives, is well reproduced by calculated results, being also very close to the value found in (**2**) compound, for which there is no experimental structural data. Also, in salicylaldehyde derivatives, O–H···N1 and C2–O–H bond angles are well reproduced by calculated results, in accordance with the inter-molecular hydrogen bond between N1 and the OH group. Torsion angle values obtained by DFT methods and, in particular, those involved in these inter-molecular hydrogen bonds, show a good agreement with those obtained by diffraction experiments.

Table 2
Selected experimental and calculated (M06-2X/6-311G(d,p)) structural parameters. See Figs. 3–5 for atom labeling and substituents nature. For compound (**1**), experimental data in the first column were extracted from Ref. 6.

	INHVa (**1**)			INHBrVa (**2**)	INHClSal (**3**)		INHBrSal (**4**)	
	Exp.[a]	Exp.[b]	Calc.	Calc.	Exp.	Calc.	Exp.	Calc.
Bond lengths (Å)								
N1···HO1	–		–	–	2.015	1.801	2.024	1.804
C2-R4	0.929	1.046	1.085	1.082	1.349	1.345	1.356	1.353
C3-R3	1.367	1.362	1.367	1.363	0.930	1.084	0.930	1.083
C4-R2	1.358	1.365	1.369	1.358	0.930	1.083	0.930	1.083
C5-R1	0.930	0.999	1.084	1.900	1.743	1.749	1.901	1.890
C13–N3	1.321	1.326	1.335	1.334	1.330	1.346	1.330	1.346
Bond angles (°)								
O–H–N1 (R4)	–	–	–	–	147.2	142.5	143.7	142.5
C–O–C3 (R3)	116.9	117.0	122.3	123.5	–	–	–	–
C2–O–H (R4)	–	–	–	–	107.3	109.3	107.8	109.4
C4–O–H (R2)	110.9	111.1	113.6	112.0	–	–	–	–
O–H (R2)–O(R3)	111.8	107.9	112.1	103.6	–	–	–	–
C1–C2–R4	120.1	120.1	120.8	121.1	123.1	123.1	123.3	123.1
C2–C3–R3	125.5	125.0	113.3	113.1	119.4	118.4	119.3	118.4
C3–C4–R2	121.4	122.8	127.3	126.3	120.2	120.3	120.6	120.1
C4–C5–R1	120.0	117.8	116.7	118.0	119.7	119.5	119.0	119.9
Torsion angles (°)								
C14–C10–C9–N2	174.1	6.69	−143.5	−141.9	163.9	140.2	−163.2	−142.1
C10–C9–N2–N1	175.5	−179.5	10.7	10.7	−177.5	−180.0	177.4	179.8
N2–N1–C8–C1	−178.3	179.6	−180.0	−179.7	−176.0	179.9	175.3	178.6
N1–C8–C1–C6	−170.5	−4.53	4.50	0.918	177.3	178.1	−177.9	−178.8
C3–C2–O–H	–	–	–	–	−176.6	−179.1	−179.9	179.7
C5–C4–O–H	178.1	−178.7	−178.6	178.3	–	–	–	–
C2–C3–O–C	11.8	−3.03	−177.4	−179.9	–	–	–	–

3.3. Vibrational spectroscopy

The infrared spectra of the compounds were measured in the 400-4000 cm^{-1} spectral range. The assignments were accomplished with the help of data obtained from Density Functional Theory calculations at the M06-2X/6–311G(d,p) level using both visualization tools and potential energy distribution analyses, taking into account the internal coordinates that mainly contribute to each calculated frequency. Recorded spectra of INH, Va and (**1**) in the most relevant spectral range, namely 1800-400 cm^{-1}, are depicted in Fig. 6. IR spectra of (**2**), (**3**) and (**4**) are included as Supplementary Material. (Figs. S1a–S1d). The analyses based on the potential energy distribution are available as Supplementary Material.

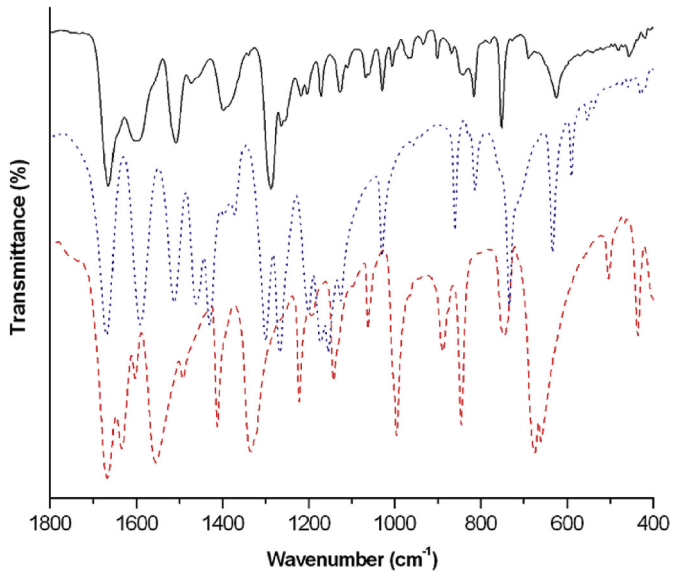

Fig. 6. Experimental IR spectra of INH (red, dashed), Va (blue, dotted) and INHVa (**1**) (black, solid) in the 1800–400 cm^{-1} spectral range. (For interpretation of the references to colour in this figure legend, the reader is referred to the web version of this article.)

In order to illustrate the behaviour in the high frequencies spectroscopic region, FTIR spectra of one hydroxialdehyde (**Va**) and one hydrazone showing protonated pyridine N atom (**3**) in the 4000–400 cm^{-1} range, are included as Supplementary Material (Figs. S1-e and S1-f, respectively).

A selection of relevant vibrational modes denoting the formation of the hydrazones are listed in Table 3, together with calculated values and proposed assignments. The complete list of vibrational modes and assignments are available as Supplementary Material Tables S3a–S3e. The assignments are in agreement with data reported previously [2,3,6–8,34,37]. Results for the already previously reported hydrazone from INH and *o*-vanillin (INHoVa) [2] are included in the Table for the purpose of comparison. For atom numbering in the following discussion see Fig. 3.

Symmetrical and unsymmetrical νH_2O modes are found in similar frequencies in all the compounds. The Ar-X (X = Cl, Br) stretching modes appear around 500 cm^{-1} for the bromine Schiff bases, while for the chlorine Schiff base are located at 715 cm^{-1}.

3.3.1. N–H vibrations

Stretching –NH vibrations of the hydrazone moiety (N2), appear in the range of 3209–3113 cm^{-1}, in agreement with the corresponding ones observed for INHoVa (3205 cm^{-1}).

It is found in the crystal structures of salicylaldehyde derivatives (**3**) and (**4**) that the pyridinic nitrogen is protonated. The broad intense band at 2517 cm^{-1} and 2410 cm^{-1}, respectively, observed for these Schiff bases can be assigned to the pyridinic N–H stretching mode. Regarding these results, we can propose that the band with similar shape at 2590 cm^{-1} in INHoVa spectra, corresponds to this mode [5]. It is worth mentioning that Malhotra et al. [37] report the (**1**) hydrazone protonated at the pyridinic nitrogen. Despite this fact, they do not report N–H vibrations.

Table 3
Selected experimental bands of the studied Schiff bases IR spectra. Values for INH and the respective aldehydes are included for comparison. Complete assignment of relevant bands and calculated frequencies are available as Supplementary Material (Tables S3a–S3e).

Assignment	INH	*o*-HVa	INHoVa	Va	INHVa (**1**)	BrVa	INHBrVa (**2**)	ClSal	INHClSa (**3**)l	BrSal	INHBrSal (**4**)
ν OH		3014 w	3014 vvw	3018 w	3020 sh	3018 vw	3037 m	3047 vw	3048 w	3042 vw	3044 w
ν N(Py)H			2590 m,b		–		–		2517 m,b		2410 m,b
ν C=O	1667 vs	1645 vs	1688 vs	1665 vs	1665 vs	1676 vs	1676 s	1663 vs	1674 vs	1672 vs	1676 vs
ν C=N			1606 vs		1599 s,b		1598 s,b		1603 s,b		1605 vs,b
δ OH		1388 s	1392 sh	1430 s	1398 m	1426 s	1418 m	1378 s	1363 m,b	1373 m	1361 m-w
νAr–OH		1327 s	1324 m-w	1300 m	1287 s	1354 s	1297 s	1304 m	1301 m	1305 mw	1301 m
ν N–N	1192 vw		1148 w		1172 m-w		1188 m		1182 w,b		1197 vw
γ OH		838 m	839 m	813 m	816 m	854 s	840 w,b	831 s	836 m-s	892 m	834 m-s
γ NH	437 w		453 vw		456 vw		454 vw		448 vw		447 vw

Unsurprisingly, the bands related to the NH_2 group in INH (at 3111, 1634 and 1321 cm^{-1}) are not present in the hydrazones spectra. A very weak band, corresponding to NH(hyd) out-of-plane deformation (γ) is found between 447 cm^{-1} and 456 cm^{-1}. The NH bending mode is found to be coupled with other modes in the hydrazones studied here and in INHoVa, showing a non-distinctive tendency along the family of compounds.

N–N stretching band, on the other hand, appears between 1172 cm^{-1} and 1197 cm^{-1} for the studied compounds, while for INHoVa and INH is at 1148 cm^{-1} and 1192 cm^{-1}, respectively.

3.3.2. O–H vibrations

The IR spectra of the studied compounds show weak bands corresponding to OH stretching modes in the 3020-3048 cm^{-1} range. Values obtained from DFT methods are much higher than the experimental ones as H-bond interactions, present in the crystal packing of the hydrazones and the aldehydes, are neglected in the calculations. This stretching vibration is observed at 3014 cm^{-1} in INHoVa Schiff base. It also remains observable at almost the same frequency after condensation for all compounds except (**2**).

Regarding δOH mode, it can be seen from the tables that it shifts to lower frequencies upon condensation for all Schiff bases. Notwithstanding, INHoVa compound shifts this mode to a higher value, from 1388 cm^{-1} in *o*-HVa to 1392 cm^{-1} in the hydrazone. With the aid of computational methods, it is also observed that this vibration is in general present in combination with other modes, making it difficult to analyze the trend in the frequency values.

Comparing the hydrazones Ar–OH stretching mode, including INHoVa, with the corresponding aldehyde, it can be appreciated from the table that it is conserved except for (**1**). This behaviour can be explained by the OH group position together with the presence of deprotonated pyridinic nitrogen atom. As can be seen in the packing of (**1**), the OH is linked to the referred N atom of a neighboring molecule by H-bond interactions, hence, leading to a red shift of this mode.

Moreover, as it was expected, computational methods underestimate OH out-of-plane deformation (γ), which is conserved in all cases, but shows a slight shift in both Va derivatives.

3.3.3. C=O and C=N stretching

The strong bands found from 1663 cm^{-1} to 1676 cm^{-1} are characteristic of the C=O stretching of the Schiff bases. It is seen that this mode is slightly blue-shifted in all the hydrazones, except for (1) in which is conserved.

A strong band is observed in the 1599–1605 cm^{-1} range, characteristic of the C=N stretching mode, which appears due to the formation of the hydrazone. Considering INHoVa [2] (C=N stretching band at 1606 cm^{-1}, see Table 3) and other related compounds [3], it can be inferred that this mode is insensitive to the nature and position of the substituents in the aldehyde ring.

In addition, it is observed that DFT calculations overestimate OH, C=O and C=N stretching modes, possibly due to the lack of restrictions in the gas phase that are present in the solid (see Supplementary Material). It must be noted that the hydrogen atom from the OH group, the oxygen atom of C=O moiety and the nitrogen atom of C=N group are all involved in H-bonds in the crystals (see Figs. 4 and 5).

3.3.4. OCH_3 vibrations

Ar–OCH_3 stretching vibrations are present as broad bands in vanillin derivatives. For (**1**) it appears at 1254 cm^{-1} and for (**2**) from 1250 cm^{-1} to 1264 cm^{-1}, coupled with other modes. It is worth mentioning that INHoVa compound has similar bands in the 1256-1283 cm^{-1} range.

Regarding CH_3 vibrations, the asymmetrical δCH_3 strong band is observed at 1510 cm^{-1} in (**1**) and at 1498 cm^{-1} in (**2**), being both in agreement with the value of 1464 cm^{-1} found for INHoVa. In the three compounds, this band is accompanied by a weak band in the 1440 cm^{-1}- 1471 cm^{-1} range, corresponding to the symmetrical mode.

3.3.5. C–H vibrations

The IR spectra of the compounds show weak bands corresponding to C8H stretching vibrations between 2842 cm^{-1} and 2926 cm^{-1} in the Schiff bases. These modes appear shifted to lower frequencies in comparison with those of the aldehydes, in most cases, except for INHoVa. Calculations overestimate frequency values in all cases.

It is also seen that symmetric and antisymmetric CH(methyl) stretching vibration modes are conserved in all hydrazones after condensation, in comparison with the same mode of the aldehyde. Calculated values of these stretching frequencies are higher than the observed ones. It is worth mentioning that these modes have a similar behaviour than those of INHoVa.

The band assigned to rings ν CH modes appear in the 3157-3050 cm^{-1} region in INHoVa; 3156-3046 cm^{-1}region in (**1**); 3148-3094 cm^{-1} region in (**2**); 3089-3027 cm^{-1} region in (**3**) and in the 3091-3017 cm^{-1} region in (**4**). It is worth noticing that for Va derivatives, the highest frequency value is originated in the aldehyde fragment, contrary to the salicylaldehyde derivatives, in which it corresponds to the INH fragment of the molecules. It is observed that the bands related to the C–H stretching mode in the hydrazide fragment are blue-shifted in comparison with those of INH. The bands corresponding to CH stretching modes in the aldehydes are overlapped with broad bands due to H_2O stretching in some cases (see Tables S3a–S3e). As a consequence, a comparison between these modes and those of the hydrazones could not be made.

3.4. NMR spectroscopy

^1H NMR and ^{13}C NMR spectra of (**2**), (**3**) and (**4**) were registered

as DMSO-d_6 solutions (see experimental section for detailed information). Selected spectral data and their assignments are listed in Table 4, together with previously reported INHoVa and (**1**) data [2,37]. Recorded spectra of compound (**4**), for which no crystal structure has been determined, are shown in Fig. 7. It can be seen, with more clarity in the ^{1}H spectrum, that signals have satellite weaker ones that conserved the ratio of integrated area with respect to the main signals. This fact could be a consequence of tautomeric equilibrium in solution.

The spectra of the hydrazones showed a signal at δ 4,92–12.95 ppm characteristics of phenolic OH proton, sensitive to their position in the ring. Calculations underestimate these chemical shifts for (**3**) and (**4**) hydrazones in wich OH···N H-bonds give rise to pseudo-rings. On the contrary, values for (**1**) and (**2**) having the OH group in *para*-possiton, are overestimated. This could be explained by considering that calculations were done for a static conformation, while in solution atoms can freely rotate along a single bond and thus, observed chemical shifts are average values of different conformations. A singlet observed at δ 8.50–8.81 ppm is assigned to the azomethine proton. The signals at δ 8.98–12.68 ppm are proposed to be due to the C═N–H hydrazine protons.

Different values observed in the protonic spectra are proposed to be due to the variation of substituents in the hydrazone's rings and to the effect of protonation or deprotonation of the pyridinic N in the molecules. It is interesting to see that despite the fact that Malhotra et al. [37] report the hydrazone to be protonated in the pyridinic nitrogen, the authors do not report the respective signal in the 1H NMR spectrum. In the case of (**3**) and (**4**) a very broad signal of difficult evaluation at δ 11 ppm approximately, can be assigned to this proton.

Besides the selected signals listed in the table, two well-defined aromatic spin systems can be observed. As expected, pyridine hydrogens appear at higher δ values than those of the phenolic ring.

Regarding the ^{13}C spectra, the presence of a peak at δ 159.81–160.1 ppm is assigned to the carbonyl carbon. The methoxy carbon is proposed to show a signal at 55.89 ppm for (**1**) and at 55.99 ppm for (**2**), both vanillin derivatives, in agreement with the reported for *o*-vanillin derivative at δ 55.87 ppm. The carbon atom linked to the OH group is, as Table 4 shows, in the 148.0–156.60 ppm range. Calculations were of aid to the assignment of the ^{13}C chemical shieldings, despite the fact that they generally overestimate values of the carbon spectra.

3.5. Electronic spectroscopy

3.5.1. Spectra analysis

The electronic absorption spectra of INH, hydroxy-aldehydes and of the hydrazones were measured in the 200–800 nm spectral range. Fig. 8 shows the electronic spectrum of the hydrazones in the most relevant spectral range, as an illustrative example. INHoVa spectrum is included for comparison.

The studied Schiff bases contain two aromatic rings, one belonging to the INH and the other to the aldehyde. For simplicity, the descriptions of the electronic transitions involving these rings are done mentioning INH or ALD referring to the respective fraction of the molecule.

Experimental absorption bands and calculated electronic transitions are listed in Table 5, together with the proposed assignments. Only those calculated electronic transitions relevant for the assignments are listed. The MO's mainly involved in the electronic transitions used to assign observed bands are available as Supplementary Material (Figs. S2a–d). It can be seen from Table 5 that the calculated transitions describe very well the experimental electronic spectra.

3.5.2. Description of the MO's involved in the transitions

For all hydrazones (see Figs. S2a–S2d), HOMO and HOMO−1 are π in character in the aldehyde ring, and non-bonding in the OH, C–N, C═O and C═N groups. In addition, they have some contributions from the different electrophilic substituents of the aldehydes, namely OCH_3 (**1**), Br [(**2**) and (**4**)] and Cl (**3**). HOMO−2 in (**3**) is non-bonding in Cl atom, the hydrazone group and oxygen atoms; it is also π in character in both INH and ALD rings. HOMO−3, involved in electronic transitions of (**2**) and (**3**), is π in character in the aldehyde ring for the salicylaldehyde derivative and in INH ring for the vanillin derivative; it is also located in oxygen and halogen atoms, C═N and C–N groups. HOMO−4 is involved in electronic transitions of (**1**), (**2**) and (**4**). In (**1**) is π in character in the aldehyde ring and it is also located in oxygen atoms, pyridinic nitrogen and hydrazone group. In (**2**), is π in character in the INH ring with some contributions from nitrogen and oxygen atoms of C═N and C═O groups. In (**4**), it is distributed among the Br atom, oxygen atoms and the hydrazone group; it is also π in character in the rings, mostly INH ring, being very similar to HOMO−6.

The LUMO is mostly π anti-bonding in the INH ring for the four hydrazones; with some contributions from oxygen atoms of the C═O group, atoms in the hydrazone moiety and ALD ring. LUMO+1 is similar to LUMO, but involving also oxygen atoms from the OCH_3, the OH group and the aldehyde ring. LUMO+2 is involved in electronic transitions of (**2**), it is π^* in character in both rings and it is also localized in Br atom and O atom of OCH_3 substituent. LUMO+3, on the other hand, participates in electronic transitions of salycilaldehyde derivatives, (**3**) and (**4**). It is π^* in character in ALD ring and non-bonding in the halogen atom, O atom of OH group and C (8). LUMO+4 is π^* in character in ALD ring of (**1**). LUMO+6 is π^* in character in both rings, with some contributions from C–N, C═N and C═O groups of (**4**).

Table 4
Selected ^{1}H and ^{13}C (500 MHz) NMR chemical shifts, in ppm, for the Schiff bases (DMSO-d_6). Calculated chemical shifts and data reported by other authors are also shown.

	INHoVa		INHVa (**1**)		INHBrVa (**2**)		INHClSal (**3**)		INHBrSal (**4**)	
	Exp. [2]	Calc. [2]	Exp. [37]	Calc.	Exp.	Calc.	Exp.	Calc.	Exp	Calc.
^{1}H										
H–O	12.46	11.56	5.08	6.15	4,92	6.50	12.98	11.48	12.95	10.78
H–C═N	8.76	8.91	8.34	8.12	8.50	7.98	8.81	8.60	8.81	8.45
H–N	–	12.48	–	–	–	–	11.07	11.26	11.11	11.21
C═N–H	10.70	10.30	11.86	8.71	12.68	8.74	8,98	9.51	9.05	9.10
^{13}C										
C═O	160.10	167.4	163.42	175.52	159.84	175.48	160.09	166.50	159.81	166.00
O–CH_3	55.87	57.19	55.89	58.67	55.99	59.05	–	–	–	–
C–OH	148.00	158.00	151.94	158.4|	148.97	154.83	155.59	168.55	156.6	166.27

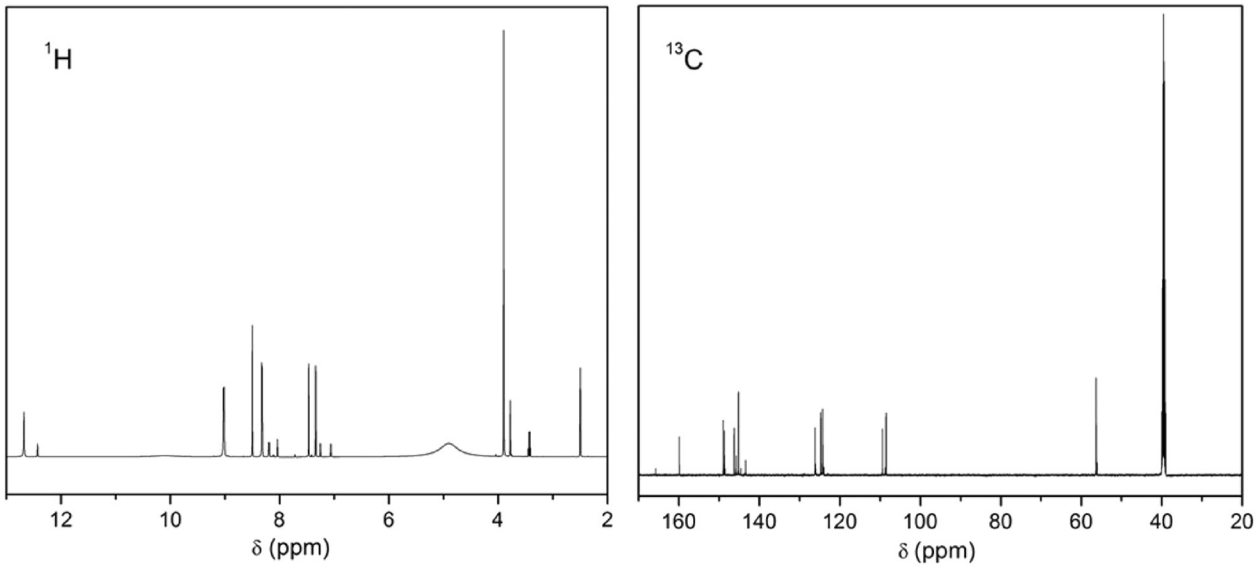

Fig. 7. ^{1}H NMR (a) and ^{13}C NMR (b) of INHBrVa (**2**) in DMSO-d_6 solution.

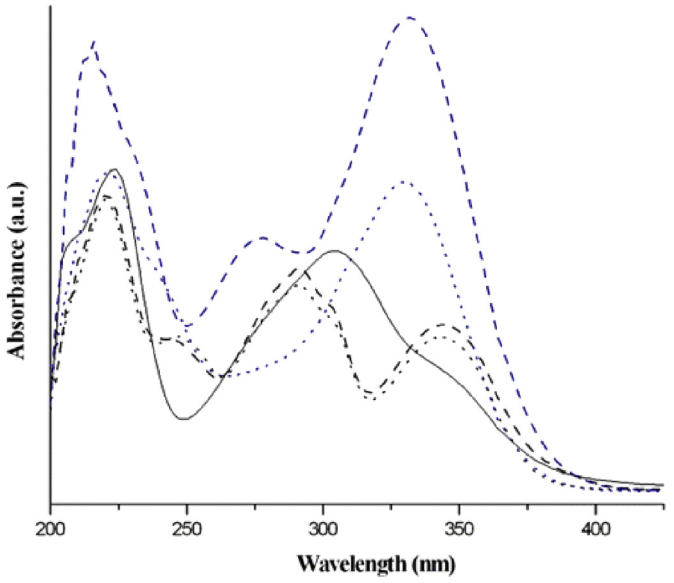

Fig. 8. Electronic absorption spectra of the hydrazones in ethanolic solution: INHVa (**1**): dashed, blue; INHBrVa (**2**), dotted, blue; INHoVa, solid black; INHClSal (**3**), dashed black and INBrSal (**4**) dotted black. (For interpretation of the references to colour in this figure legend, the reader is referred to the web version of this article.)

3.5.3. Electronic absorption spectrum of INHVa (*1*)

According to the above description and the data from Table 5, the observed shoulder at 208 nm is calculated at 210 nm and mainly assigned to a π → π* transition from ALD ring to the INH ring. The observed band at 214 nm, which is calculated at 215 nm, is proposed to be due to a transition involving ALD ring, with some contributions of C–N and C=N groups. A π → π* electronic transition mainly from ALD ring to INH ring and with minor contributions from C=N, C=O and OH groups is calculated at 240 nm to describe the observed shoulder at 232 nm. Two close electronic transitions calculated at 280 nm and 289 nm, correspond to the band measured at 276 nm; this band is due to π → π* transitions from the ALD fragment of the molecule to the INH one, involving also OH, C–N, C=N and OCH_3 groups. The band observed at 332 nm is calculated at 328 nm and assigned mostly to a π → π* transition from ALD ring to the INH ring.

Table 5
Electronic absorption spectra of 3×10^{-5} M ethanolic solutions of the studied isonicotinoyl hydrazones. Results from TD-DFT are also shown. Percentage contributions of calculated transitions are given in parentheses. Absorption maxima are given in nm. Oscillator strengths, shown in parenthesis, are in a.u.

Exp.	Calc.	Assignment
INHVa (1)		
208 sh	210 (0.0485)	HOMO − 4 → LUMO + 1 (72%)
214	215 (0.1011)	HOMO − 1 → LUMO + 4 (61%)
232 sh	240 (0.6052)	HOMO → LUMO + 4 (31%)
		HOMO − 1 → LUMO + 1 (55%)
276	280 (0.2491)	HOMO − 1 → LUMO (58%)
	289 (0.1193)	HOMO → LUMO + 1 (85%)
332	328 (0.3620)	HOMO → LUMO (98%)
INHBrVa (2)		
210 sh	215 (0.0802)	HOMO − 3 → LUMO + 1 (34%)
		HOMO − 1 → LUMO + 2 (34%)
222	219 (0.1027)	HOMO − 4 → LUMO + 1 (29%)
		HOMO − 3 → LUMO + 1 (23%)
	235 (0.1369)	HOMO − 1 → LUMO + 1 (23%)
		HOMO → LUMO + 1 (20%)
242 sh	240 (0.2914)	HOMO → LUMO +2 (33%)
		HOMO − 3 → LUMO (20%)
	241 (0.1885)	HOMO → LUMO + 2 (56%)
307 sh	278 (0.2373)	HOMO − 1 → LUMO + 1 (88%)
330	316 (0.4116)	HOMO → LUMO (98%)
INHClSal (3)		
210 sh	210 (0.1039)	HOMO − 2 → LUMO + 3 (20%)
220	231 (0.3940)	HOMO → LUMO + 3 (76%)
246	245 (0.0265)	HOMO − 3 → LUMO (84%)
292	260 (0.4151)	HOMO − 1 → LUMO + 1 (83%)
303 sh	307 (0.1913)	HOMO → LUMO + 1 (93%)
345	404 (0.1661)	HOMO → LUMO (98%)
INHBrSal (4)		
208 sh	212 (0.2034)	HOMO − 1 → LUMO + 3 (39%)
		HOMO → LUMO + 6 (38%)
220	234 (0.4460)	HOMO → LUMO + 3 (76%)
248	239 (0.1112)	HOMO − 6 → LUMO (63%)
291	260 (0.4147)	HOMO − 1 → LUMO + 1 (83%)
304 sh	308 (0.1668)	HOMO → LUMO + 1 (94%)
344	407 (0.1580)	HOMO → LUMO (98%)

sh = shoulder.

*3.5.4. Electronic absorption spectrum of INHBrVa (**2**)*

The bands are assigned on the basis of the description of the MO's and the data of Table 5. The shoulder observed at 210 nm is calculated at 215 nm and assigned mostly to a $\pi \rightarrow \pi^*$ transition involving INH ring with minor non-bonding contributions from Br atom, oxygen atoms and C–N and C=N groups. The band at 222 nm is described by two calculated transitions, one at 219 nm and the other at 235 nm; it is assigned to $\pi \rightarrow \pi^*$ transitions from both aromatic rings to INH ring. The shoulder at 242 nm is also described by two calculated values, at 240 nm and at 241 nm; it is assigned to $\pi \rightarrow \pi^*$ transitions involving both rings, with minor contributions from the electrophilic substituents of the aldehydes. The shoulder found at 307 nm and the band at 330 nm are calculated at 278 nm and 316 nm, respectively. These bands are assigned to $\pi \rightarrow \pi^*$ transitions from ALD ring to the INH ring, with minor contributions from OH, C–N, C=O and C=N groups.

*3.5.5. Electronic absorption spectrum of INHClSal (**3**)*

On account of the provided descriptions of the MO's and the electronic spectra described in Table 5, the shoulder observed at 210 nm is mainly assigned to an electronic transition from both rings of (**3**) to the ALD fragment of the molecule, including non-bonding contributions of its substituents. The band at 220 nm is calculated at 231 nm and assigned to a $\pi \rightarrow \pi^*$ transition in the ALD ring and its substituents. The band at 246 nm is due to a $\pi \rightarrow \pi^*$ transition from ALD ring to INH ring, with some contributions of nitrogen and chlorine atoms. The band at 292 nm and the shoulder at 303 nm are calculated at 260 nm and 307 nm, respectively; they are assigned to electronic transitions from ALD ring to both rings with contributions from Ar–C, C–N and C=N bonds. Interestingly, chlorine atom is not involved. The band measured at 345 nm is calculated at 404 nm and assigned to a $\pi \rightarrow \pi^*$ transition from ALD ring and substituents to INH ring, with minor contributions from C–N and C=N bonds, OH group and oxygen atom from C=O.

*3.5.6. Electronic absorption spectrum of INHBrSal (**4**)*

According to the analysis of the MO's and the data from Table 5, the shoulder at 208 nm can be mainly assigned to one transition in ALD ring and its substituents, with minor contributions from oxygen and nitrogen atoms; and to another from ALD ring to both rings, C and O atom from C=O group and nitrogen atom form hydrazone group. The band at 220 nm, calculated at 234 nm, is assigned to $\pi \rightarrow \pi^*$ transitions in ALD ring, with non-bonding contributions from bromine, oxygen and nitrogen atoms. The band found at 248 nm, is calculated at 239 nm and assigned to $\pi \rightarrow \pi^*$ transitions in both ALD and INH rings, with non-bonding contributions from bromine, oxygen and nitrogen atoms. The shoulders at 280 nm and 304 nm are assigned to transitions from ALD ring, including its substituents, to both rings with minor contributions from nitrogen atoms. The band at 291 nm is calculated at 293 nm and assigned mainly to a transition from both rings, bromine and oxygen atom from C=O, to INH ring. The band at 344 nm is described by two calculated values, one at 333 nm and the other at 407 nm; it is assigned to a $\pi \rightarrow \pi^*$ transition from ALD ring to INH ring, with minor contributions from bromine, nitrogen and oxygen atoms.

3.6. A theoretical analysis of the reactivity of the hydrazones

The interesting application of hydrazones as good chelating agents, has been extensively studied (see Ref. [1] and references therein). This capacity arises from the available electronic density in the –C=N–N–C=O group, suitable for metal coordination [5].

Furthermore, it has been stated before [38] that HOMO energies (E_H) are associated with the electron donating ability of a molecule. In particular, high values (that is, less negative ones) of E_H are likely to indicate a tendency of a molecule to donate electrons to appropriate receptors, such as transition metals. Thus, E_H could indicate the tendency of ligands to coordinate such metals.

On the other hand, the LUMO energy, E_L, is equivalent to electron affinity, according to Koopmans' theorem [39]. Moreover, LUMO energies are also associated with electron transfer rates [38]. Regarding the well-known anti-oxidant properties of this kind of ligands, often enhanced upon metal complex formation, the analysis of the electron affinity gains interest. This property has been employed to account for the electron transfer rate from superoxide anion to copper atom [40–42]. The lower the electron affinity (that is, less negative values of E_L), the higher the electron transfer rate, leading to higher superoxide radical scavenging activity, being the superoxide dismutase-mimic activity one of the main interests in this kind of copper complexes. To gain more insight into the reactive behaviour of this family of hydrazones, we calculated these properties, which are listed in Table 6.

It can be seen in Table 6 that the E_H values of the vanillin hydrazone, (**1**), and the salicylaldehyde derivatives (**3**) y (**4**) are the less negative ones and, moreover, they are close each other. Thus, they would be better candidates to form complexes with metal ions than the hydrazine (**2**). It is interesting to note from Figs. 2 and 3 that the OH group is in *para* position in vanillin derivatives, whereas it is in *ortho* position in the salicylaldehyde derivatives. The OH group in *ortho* position, together with the azomethine group, might favour the role of polydentate chelating agent for salicylaldehyde derivatives. Therefore, it is proposed that (**3**) and (**4**) hydrazones would be better candidates to form complexes with metal ions than (**1**) or (**2**). Therefore, we propose that hydrazones (**3**) and (**4**) would have a better chance of being chelated than (**1**) or (**2**).

Calculated E_L values, shown in Table 6, indicate that (**1**) would have the highest superoxide radical scavenging activity of the studied hydrazones, closely followed by (**2**).

MEP-derived atomic charges (ESP charges, from now on) can be a useful index to identify potential sites for coordination with metals, as they predict possible sites for nucleophilic or electrophilic attacks [43]. We calculated them, in an attempt to identify these reactivity sites, as we have already done in previous work [44]. Selected ESP charges of the compounds are listed in Table 7.

It can be seen from the table that the oxygen atoms belonging to OH and C=O groups present large negative ESP charges for all the molecules under study suggesting that they are prone to undergo electrophilic attacks. It is interesting to note that although the oxygen atom in the OCH_3 group exhibits a small negative ESP charge, it could participate in the coordination sphere of a complex together with the oxygen atom from the OH group, as it was determined in the vanillin-copper complex [45]. Also, both nitrogen atoms in the –C=N–N–C=O moiety seem to be good candidates for an electrophilic attack, although N2 presents a considerably most negative ESP charge than N1. As expected, N3 shows a small negative charge when is protonated in ClSal and BrSal Schiff bases, whereas large negative charges are found for that atom in (**1**) and (**2**), in which it is not protonated. The pyridinic

Table 6
HOMO (E_H) and LUMO (E_L) energies (in eV) for the hydrazones, calculated at the M06-2X/6–311G(d,p) level of theory.

	E_H	E_L
INHVa (**1**)	−6.49	−1.05
INHBrVa (**2**)	−7.31	−1.45
INHClSal (**3**)	−6.70	−3.11
INHBrSal (**4**)	−6.70	−3.11

Table 7
MEP-derived atomic charges of selected atoms, in units of |e|, at the M06-2X/6–311G(d,p) level of theory. See Fig. 3 for atom numbering and structures.

	INHVa (**1**)	INHBrVa (**2**)	INHClSal (**3**)	INHBrSal (**4**)
O (OH)	−0.5029	−0.5029	−0.5691	−0.5680
O (OCH_3)	−0.2436	−0.2497	–	–
N1	−0.2285	−0.1780	−0.1393	−0.1265
N2	−0.3222	−0.3453	−0.4125	−0.4131
N3	−0.6601	−0.6379	−0.1761	−0.1534
O (C=O)	−0.5134	−0.5057	−0.4591	−0.4572
Br1	–	−0.0307	–	−0.0196
Cl1	–	–	−0.0679	–

nitrogen atom could participate in a coordination compound, forming complex structures, as it was reported previously [46]. These findings agree with those found above when the magnitude of E_H was correlated with the ability of the molecules under study to form complexes.

4. Conclusions

Four hydrazones derived from isoniazid (INH), a well-known antituberculous agent, were prepared. They were obtained with good yield upon condensation with a group of hydroxybenzaldehydes, namely *Va, BrVa, ClSal, BrSal*.

The crystal structures of three of them were determined and compared with reported data for the related Schiff base INHoVa. Hydrazones (**3**) and (**4**) are isomorphic and chiral counterparts of each other. Structure of compound (**1**) differs from the already reported by other authors, probably as an effect of the crystallization rate during the synthesis process.

DFT-based calculations carried out on the family of compounds showed a very good agreement with experimental data. These results were of relevance in the interpretation and assignment of the bands in the spectroscopic analysis. The few cases in which the calculated values differed significantly from the experimental results were attributed to molecular interactions which were neglected in the calculations. Moreover, calculated geometrical parameters are in very good agreement with experimental data, even in the cases involving atoms that participate in intermolecular H-bonds.

The FT-IR of solid samples and UV–vis of ethanol solutions spectra of the four hydrazones were recorded together with those of INH and the respective aldehydes. They were analyzed and discussed in comparison with INHoVa hydrazone. The vibrational behaviour is in perfect accordance with the expected for azomethine moiety formation and the observed crystallographic details. Strong coupling among different modes was observed in the assignment of various bands.

The effect of the nature and location of substituent groups in the ring and of protonation or deprotonation of the pyridinic N atom are also evidenced in the ^1H and ^{13}C NMR spectra.

In the electronic spectra the bands predicted in the calculations for the hydrazones could be observed and assigned. In most cases, more than one electronic transition was involved in each signal.

The calculation of some reactivity properties indicate that the Schiff bases (**3**) and (**4**) are good candidates to act as polydentate ligands in the formation of coordination compounds. On the other hand, the vanillin hydrazone (**1**) shows the highest superoxide radical scavenging activity, calculated as the energy of the LUMO, which could be related to electron transfer processes present in superoxide radical anion dismutation.

Acknowledgments

This work was supported by CONICET (CCT-La Plata), UNLP and ANPCyT, Argentina. G.A.E., O.E.P., R.P.D. and A.C.G.B. are members of the Research Career of CONICET. The authors thank Christian D. Alcívar León (CEQUINOR-CONICET-UNLP) for his help with the NMR spectra.

Appendix A. Supplementary material

Supplementary material related to this article can be found at http://dx.doi.org/10.1016/j.molstruc.2016.12.018.

References

[1] X. Xu, I. Aprahamian, Chem. Soc. Rev. 43 (2014) 1963–1981.
[2] A.C. González-Baró, R. Pis-Diez, B.S. Parajón-Costa, N.A. Rey, J. Mol. Struct. 1007 (2012) 95–101.
[3] V. Ferraresi-Curotto, G.A. Echeverría, O.E. Piro, R. Pis-Diez, A.C. Gonzalez-Baró, Spectrochim. Acta Part A 137 (2015) 692–700.
[4] E.F. Oga, Int. J. Pharm. Pharm. Sci. 2 (2010) 55–58.
[5] D. Cook, Can. J. Chem. 39 (1961) 2009–2024.
[6] X.F. Shi, L. He, G.Z. Ma, C.C. Yuan, Acta Cryst. E 63 (2007) o1119.
[7] M.R. Maurya, S. Khurana, C. Schulzke, D. Rehder, Eur. J. Inorg. Chem. (2001) 779–788.
[8] R. Manikandan, P. Viswanathamurthi, M. Muthukumar, Spectrochim. Acta Part A 83 (2011) 297–303.
[9] CrysAlisPro, Oxford Diffraction Ltd. version 1.171.33.48 (release 15-09-2009 CrysAlis171.NET).
[10] G.M. Sheldrick, Acta Cryst. A 64 (2008) 112–122.
[11] H.D. Flack, Acta Cryst. A 39 (1983) 876–881.
[12] J.J.P. Stewart, J. Mol. Model 13 (2007) (2012) 1173–1213. MOPAC2012; James J.P. Stewart, Stewart Computational Chemistry, Colorado Springs, CO, USA, http://OpenMOPAC.net.
[13] Y. Zhao, D.G. Truhlar, Theor. Chem. Acc. 120 (2008) 215–241.
[14] R. Krishnan, J.S. Binkley, R. Seeger, J.A. Pople, J. Chem. Phys. 72 (1980) 650–654.
[15] T. Clark, J. Chandrasekhar, P.V.R. Schleyer, J. Comput. Chem. 4 (1983) 294–301.
[16] V. Barone, M. Cossi, J. Phys. Chem. A 102 (1998) 1995–2001.
[17] M. Cossi, N. Rega, G. Scalmani, V. Barone, J. Comput. Chem. 24 (2003) 669–681.
[18] A. Dreuw, M. Head-Gordon, Chem. Rev. 105 (2005) 4009–4037.
[19] P. Elliott, F. Furche, K. Burke, Rev. Comp. Chem. 26 (2009) 91–165.
[20] C. Adamo, V. Barone, J. Chem. Phys. 110 (1999) 6158–6170.
[21] M.W. Schmidt, K.K. Baldridge, J.A. Boatz, S.T. Elbert, M.S. Gordon, J.H. Jensen, S. Koseki, N. Matsunaga, K.A. Nguyen, S.J. Su, T.L. Windus, M. Dupuis, J.A. Montgomery, J. Comput. Chem. 14 (1993) 1347–1363.
[22] J.R. Cheeseman, G.W. Trucks, T.A. Keith, M.J. Frisch, J. Chem. Phys. 104 (1996) 5497–5509.
[23] R. Ditchfield, J. Mol. Phys. 27 (1974) 789–807.
[24] K. Wolinski, J.F. Hinton, P.J. Pulay, J. Am. Chem. Soc. 112 (1990) 8251–8260.
[25] J. Tomasi, B. Mennucci, E. Cancès, J. Mol. Struct. THEOCHEM 464 (1999) 211–226.
[26] M.J. Frisch, G.W. Trucks, H.B. Schlegel, G.E. Scuseria, M.A. Robb, J.R. Cheeseman, J.A. Montgomery Jr., T. Vreven, K.N. Kudin, J.C. Burant, J.M. Millam, S.S. Iyengar, J. Tomasi, V. Barone, B. Mennucci, M. Cossi, G. Scalmani, N. Rega, G.A. Petersson, H. Nakatsuji, M. Hada, M. Ehara, K. Toyota, R. Fukuda, J. Hasegawa, M. Ishida, T. Nakajima, Y. Honda, O. Kitao, H. Nakai, M. Klene, X. Li, J.E. Knox, H.P. Hratchian, J.B. Cross, V. Bakken, C. Adamo, J. Jaramillo, R. Gomperts, R.E. Stratmann, O. Yazyev, A.J. Austin, R. Cammi, C. Pomelli, J.W. Ochterski, P.Y. Ayala, K. Morokuma, G.A. Voth, P. Salvador, J.J. Dannenberg, V.G. Zakrzewski, S. Dapprich, A.D. Daniels, M.C. Strain, O. Farkas, D.K. Malick, A.D. Rabuck, K. Raghavachari, J.B. Foresman, J.V. Ortiz, Q. Cui, A.G. Baboul, S. Clifford, J. Cioslowski, B.B. Stefanov, G. Liu, A. Liashenko, P. Piskorz, I. Komaromi, R.L. Martin, D.J. Fox, T. Keith, M.A. Al-Laham, C.Y. Peng, A. Nanayakkara, M. Challacombe, P.M.W. Gill, B. Johnson, W. Chen, M.W. Wong, C. Gonzalez, J.A. Pople, Gaussian 03, Revision D.01, Gaussian, Inc., Wallingford CT, 2004.
[27] A.R.J. Allouche, Comput. Chem. 32 (2011) 174–182.
[28] B.M. Bode, M.S. Gordon, J. Mol. Graph. Model 16 (1998) 133–138.
[29] http://info.ifpan.edu.pl/~kisiel/vibr/vibr.htm.
[30] Marvin 6.2.2, ChemAxon, 2014. http://www.chemaxon.com.
[31] L.J. Farrugia, J. Appl. Cryst. 30 (1997) 565.
[32] Z. Shafiq, M. Yaqub, M.N. Tahir, A. Hussain, M.S. Iqbal, Acta Cryst. E 65 (2009) o2899.
[33] X. Liu, X.-F. Shi, Acta Cryst. E 63 (2007) o4807.
[34] W. Kabsch, Acta Cryst. A 32 (1976) 922–923.
[35] T. Sedaghat, M. Yousefi, G. Bruno, H.A. Rudbari, H. Motamedi, V. Nobakht, Polyhedron 79 (2014) 88–96.

[36] D.S. Yang, Acta Cryst. E 62 (2006) o3755.
[37] M. Malhotra, G. Sharma, A. Deep, A. Pol, Pharm. Drug Res. 69 (2012) 637–644.
[38] M. Behpour, S.M. Ghoreishi, N. Mohammadi, N. Soltani, M. Salvati-Niasari, Corros. Sci. 52 (2010) 4046–4057.
[39] T.A. Koopmans, Physica 1 (1933) 104–113.
[40] H.F. Ji, H.Y. Zhang, Chem. Res. Toxicol. 17 (2004) 471–475.
[41] H.F. Ji, H.Y. Zhang, Bioorg. Med. Chem. Lett. 15 (2005) 21–24.
[42] L. Shen, H.Y. Zhang, H.F. Ji, J. Mol. Struct. (THEOCHEM) 817 (2007) 161–162.
[43] P. Politzer, J.S. Murray, in: K.B. Lipkowitz, D.B. Boyd (Eds.), Reviews in Computational Chemistry, vol. 2, John Wiley & Sons, Inc., Hoboken, NJ, USA, 1991, pp. 273–312.
[44] V. Ferraresi-Curotto, G.A. Echeverría, O.E. Piro, R. Pis-Diez, A.C. Gonzalez-Baró, Spectrochim. Acta Part A 118 (2014) 279–286.
[45] B. Kozlevćar, B. Mušič, N. Lah, I. Leban, P. Šegedin, Acta Chim. Slov. 52 (2005) 40–43.
[46] S. Naskar, M. Corbella, A.J. Blake, S. Kumar Chattopadhyay, Dalton Trans. (2007) 1150–1159.